Raman scattering in $K_{1-x}Rb_xAlF_4$: evidence of a new phase

1993 J. Phys.: Condens. Matter 5 3177

(http://iopscience.iop.org/0953-8984/5/19/016)

J. Phys.: Condens. Matter 5 (1993) 3177–3192. Printed in the UK

Raman scattering in $K_{1-x}Rb_xAlF_4$: evidence of a new phase

M Papin, A Bulou and J Nouet

Laboratoire PEC, URA CNRS No 807, Faculté des Sciences, Université du Maine, Avenue O Messiaen, 72017 Le Mans Cedex, France

Received 10 August 1992

Abstract. A Raman scattering study of the quasi-reversible structural phase transitions observed below room temperature in the perovskite-type layer compounds $K_{1-x}Rb_xAlF_4$ with $x = 0.06$, 0.09 and 0.15 is reported. The Raman spectra were analysed with the help of the result of a calculation of the phonon spectrum in the ideal (aristotypic) phase (phase I, $P4/mmm$ symmetry). For all the studied compounds, the spectra collected at room temperature are consistent with the $P4/mbm$ symmetry (phase II), resulting from the condensation of the M_3 mode. The phase IIIa Raman spectra for $x = 0.06$ and $x = 0.09$ are explained with the $P2_1/m$ space group and the phase II–phase IIIa transition can be imputed to the condensation of two components of the degenerate X_3^1 mode plus one of the components of the degenerate M_5^1 mode. The Raman spectra of the $K_{0.85}Rb_{0.15}AlF_4$ compound, on lowering the temperature, reveal the existence of a new phase (IIIb) between phase II and phase IIIa. An assignment to vibrational modes, in this phase IIIb, is possible in the $Pmmn$ space group and so the phase IIIa–phase IIIb transition could be attributed to the condensation of the X_3^1 mode like in pure $RbAlF_4$. The non-reversible martensitic phase transition of the pure compound $KAlF_4$ is no longer observed for $x = 0.15$.

1. Introduction

The structures of the tetrafluoroaluminates $AAlF_4$ with A=Tl, Rb, K, $K_{1-x}Rb_x$ derive from the ideal (or aristotypic) tetragonal structure made of AlF_6 octahedra centred on a square-base parallelepiped lattice of cations [1] (figure 1). All these quasi-two-dimensional compounds undergo several structural phase transitions (STP). Two of them, $RbAlF_4$ and $KAlF_4$, have been widely studied. Below room temperature, the former exhibits a second-order displacive SPT [2] whereas the latter (isostructural) presents a martensitic SPT [3] with a break-up of the crystal. According to the behaviour of the phonon spectrum, the martensitic phase transition in $KAlF_4$ could be explained as the result of a displacive SPT leading to an unstable phase [4]. To have a better understanding of this transition, a study of $K_{1-x}Rb_xAlF_4$ compounds has been undertaken in order to check if the Rb ions could stabilize the phase resulting from the condensation of the mode that is supposed to be responsible for the martensitic transition. The first work carried out by diffraction for $x = 0$ to $x = 0.09$ [5] revealed that the temperature of the martensitic phase transition decreases substantially with x ($\Delta T \simeq 10\,°C/\%$) and that for x greater than 2% it is preceded by an additional SPT. This new phase transition, quasi-reversible, could be interpreted as coming from condensation of two modes at two different points of the Brillouin zone.

The present work is devoted to the study of these SPT by Raman scattering. The concentrations investigated have been extended to 15%, which seems to be the limit to obtain single crystals with good optical quality and with dimensions large enough to perform

0953-8984/93/193177+16$07.50

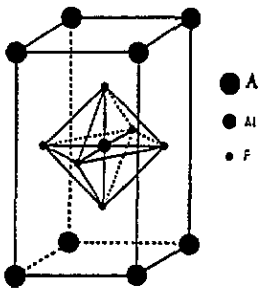

Figure 1. Tetragonal cell of the aristotypic structure of the tetrafluoroaluminates $AAlF_4$ with A=K, Rb, Tl, NH_4.

macro-Raman studies. The extension of the concentration range with regard to the preceding work reveals the existence of a new SPT and makes it possible to establish the phase diagram for rubidium concentration between 0 and 15% as reported in figure 2.

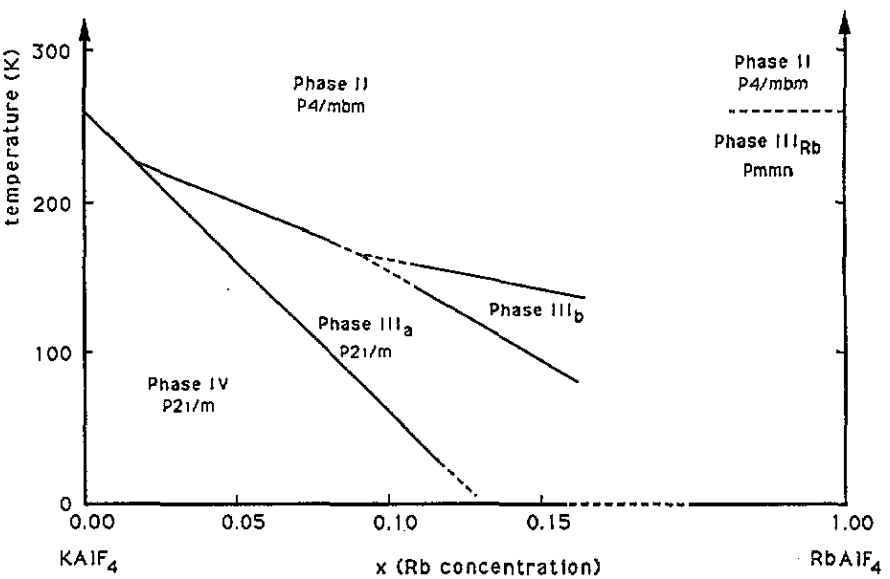

Figure 2. Schematic phase diagram of the system $KAlF_4$–$RbAlF_4$.

2. Experimental procedure

$K_{1-x}Rb_xAlF_4$ (*with* $x = 0.06$, *0.09 and 0.15*) *single crystals were grown by the Bridgman* method and were oriented by Laue back-reflection x-ray photographs. Crystals were cut with faces perpendicular to the [1 0 0], [0 1 0] and [0 0 1] directions of the ideal high-temperature phase I.

The Raman scattering spectra were recorded with a Dilor Z24 Raman spectrometer. The 514.5 nm line of an argon-ion laser (Coherent Innova 90.3) was used as the exciting source.

Low-temperature measurements, down to 50 K, were performed with a closed-cycle refrigerator.

3. Results

3.1. Preliminaries

$RbAlF_4$ presents the ideal structure (denoted phase I) at high temperature with cell parameters a_I, b_I, c_I. Using Glazer's notation [6], this structure can be labelled $a^0a^0c^0$ according to its octahedra network. On lowering the temperature, it undergoes two structural phase transitions at $T_{c1} = 553$ K and at $T_{c2} = 282$ K. Below T_{c1} (phase II), the AlF_6 octahedra are tilted around the tetragonal c_I axis, which can be described by the $a^0a^0c^+$ system. The space group is $P4/mbm$ with a unit cell $a_{II} = a_I + b_I$, $b_{II} = -a_I + b_I$, $c_{II} = c_I$ [7]. Below T_{c2} (phase III_{Rb}), the AlF_6 octahedra undergo two additional rotations around the [1 0 0] and [0 1 0] axes of the ideal structure (and a simultaneous translation of Rb^+ ions along the [0 0 1] direction). The tilt system can be summarized by the $a_p^+b_p^+c^+$ extended Glazer's notation [2], where the additional subscript p means parallel tilts of successive octahedra along the [0 0 1] direction. The space group is $Pmmn$ with a unit cell $a_{III} = 2a_I$, $b_{III} = 2b_I$, $c_{III} = c_I$ [2]. These SPT have been shown to be displacive: they respectively arise from condensation of soft modes at the M point (M_3 symmetry mode) and the X point (X_3 symmetry mode) of the ideal tetragonal Brillouin zone [8,9].

$KAlF_4$ has at room temperature the same structure as $RbAlF_4$ denoted phase II ($KAlF_4$ does not exist in the ideal phase, as the transition would occur above the melting point). At low temperature, it undergoes a martensitic-like transition to a phase denoted IV at $T_{II-IV} = 260$ K. This new phase mainly comes from an $a_I/2$ gliding of the AlF_4 octahedra sheets. The space group becomes $P2_1/m$. The structure of this phase IV derives from the orthorhombic ideal structure of $KFeF_4$ [3, 10]. In the $KAlF_4$ phonon spectrum, a nearly flat phonon branch setting between M and X points of the ideal Brillouin zone is observed and its frequency softens when the martensitic transition is approached. It has been concluded that the transition is probably connected with a displacive mechanism [4, 8].

The partial substitution of K by Rb atoms results in a decrease of T_{II-IV} and the appearance of a new intermediate phase III, setting between T_{II-III} and T_{III-IV}, for rubidium content $0.02 \leqslant x \leqslant 0.1$. This new phase determined by neutron powder diffraction for $K_{0.97}Rb_{0.03}AlF_4$ can be described again by AlF_6 octahedra rotations: it corresponds to the $a_p^-b_p^+c^+$ system according to the extended Glazer's notation. The a_{III}, b_{III} and c_{III} cell parameters are such that $a_{III} = 2a_I$, $b_{III} = 2b_I$, $c_{III} = c_I$ and the space group is $P2_1/m$ [5].

In the present work, the Raman spectra are studied on the basis of group theory analysis together with a comparison with the vibrational spectrum calculated in the ideal phase of pure $KAlF_4$ [8] and the compatibility relations between the different phases. Such an approach is based on the fact that the frequencies of the vibrational modes are not strongly sensitive to phase transition except for the (soft) mode whose condensation is responsible for the transition.

3.2. Phase II

The Raman spectra of all the studied materials present the same characteristics at room temperature (figure 3). It is reasonable to think that the room-temperature structure of these mixed compounds (with $x \leqslant 0.15$) is identical to the $KAlF_4$ or $RbAlF_4$ structure with the $P4/mbm$ space group.

The group theoretical analysis of the normal modes of vibration at the Γ point (Brillouin-zone centre) has been performed by the factor group method based on the ionic positions. Seven Raman-active modes are predicted with the following symmetries:

$$2A_{1g} + B_{1g} + B_{2g} + 3E_g.$$

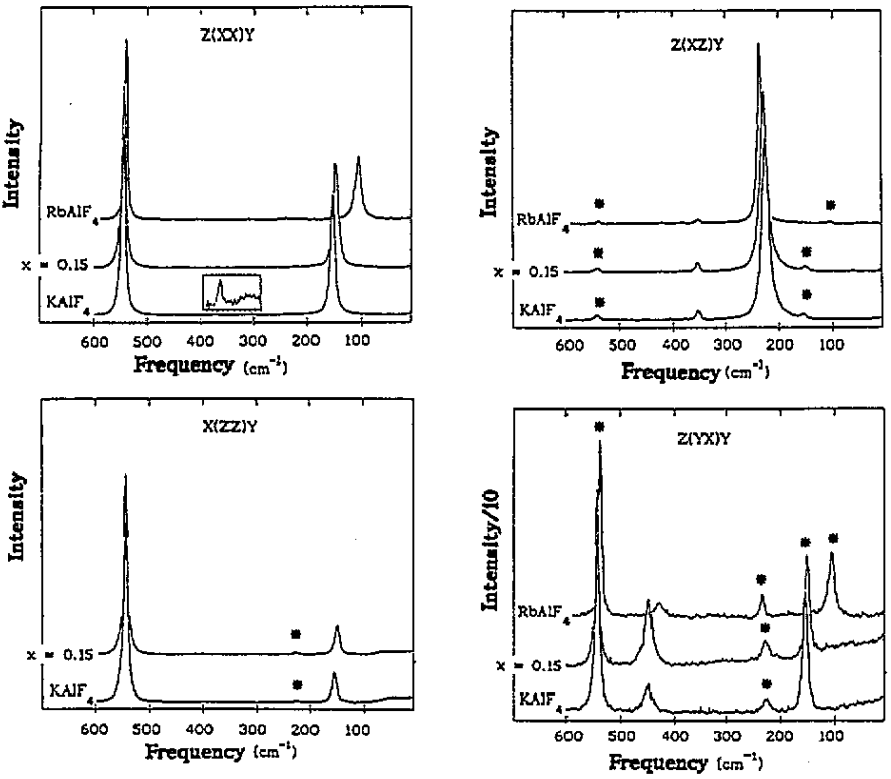

Figure 3. Raman spectra of $KAlF_4$, $RbAlF_4$ and $K_{0.85}Rb_{0.15}AlF_4$ collected at room temperature in the $Z(XX)Y$, $X(ZZ)Y$, $Z(XZ)Y$ and $Z(YX)Y$ geometries. Asterisks indicate contamination due to intense lines active in another geometry.

In the following, the diffusion geometry (X, Y, Z) for the analysis of the Raman polarization is labelled with respect to the crystallographic axes of the aristotypic phase $(\boldsymbol{a}_I, \boldsymbol{b}_I, \boldsymbol{c}_I)$. The geometry required to observe these modes can be deduced from table 1. Note that with the system of axes X, Y, Z chosen (which is 45° rotated around the tetrad axis with respect to the crystallographic axes of phase II), the B_{1g} line corresponds to the YX geometry while the B_{2g} one corresponds to XX and YY geometries.

For the discussion, we will refer to the frequencies measured and calculated in $KAlF_4$.

The A_{1g} (XX, YY, ZZ geometries) spectra recorded at room temperature exhibit two strong lines (figure 3) at 156 and 544 cm^{-1}. A low-intensity mode is also observed at 374 cm^{-1} in XX (or YY) geometry and not detected in ZZ polarization. Thus, the lines at 156 and 544 cm^{-1} correspond to A_{1g} modes and the line measured at 374 cm^{-1} comes from a B_{2g} mode (table 1).

In the XZ (or YZ) geometries, four lines are observed. Two of them come from contamination by the (intense) A_{1g} lines. They are indicated by asterisks in figure 3. Hence two E_g symmetry modes are observed at 228 and 354 cm^{-1}.

In the YX geometry, only the line at 451 cm^{-1} corresponds to a B_{1g} mode. The others come from contamination due to the strong A_{1g} and E_g lines.

These frequencies can be compared with the values calculated in phase I for pure $KAlF_4$ with a rigid-ion model. The 10 parameters of the rigid-ion model were refined from

Table 1. Raman polarizability tensors corresponding to Raman-active modes of $K_{1-x}Rb_xAlF_4$ in a system of axes (X, Y, Z) labelled with respect to the crystallographic axes of the ideal phase I and taking into account possible domains.

	Phase II P4/mbm	Phase III_{Rb} Pmmn	Phase III(or III_a) $P2_1/m$
A_{1g}	$\begin{bmatrix} a & . & . \\ . & a & . \\ . & . & b \end{bmatrix}$	A_g $\begin{bmatrix} a & . & . \\ . & b & . \\ . & . & c \end{bmatrix}$	A_g $\begin{bmatrix} c & . & . \\ . & a & d \\ . & d & b \end{bmatrix}$ X//C_2
B_{1g}	$\begin{bmatrix} . & c & . \\ c & . & . \\ . & . & . \end{bmatrix}$	B_{1g} $\begin{bmatrix} . & d & . \\ d & . & . \\ . & . & . \end{bmatrix}$	B_g $\begin{bmatrix} . & e & f \\ e & . & . \\ f & . & . \end{bmatrix}$
B_{2g}	$\begin{bmatrix} d & . & . \\ . & -d & . \\ . & . & . \end{bmatrix}$	B_{2g} or B_{3g} $\begin{bmatrix} . & . & e \\ . & . & . \\ e & . & . \end{bmatrix}$	A_g $\begin{bmatrix} b & . & d \\ . & c & . \\ d & . & a \end{bmatrix}$ Y//C_2
E_g	$\begin{bmatrix} . & . & -e \\ . & . & e \\ -e & e & . \end{bmatrix}$	B_{3g} or B_{2g} $\begin{bmatrix} . & . & . \\ . & . & f \\ . & f & . \end{bmatrix}$	B_g $\begin{bmatrix} . & f & . \\ f & . & e \\ . & e & . \end{bmatrix}$
	$\begin{bmatrix} . & . & -e \\ . & . & -e \\ -e & -e & . \end{bmatrix}$		

the frequencies of the A_{1g} mode at 544 cm^{-1}, the E_g mode at 228 cm^{-1}, the acoustic velocities and some low-frequency zone boundary modes determinated by inelastic neutron scattering [8]. The calculated frequencies are reported in table 2. Phase II results from a (virtual) phase transition arising from the condensation of a mode located at the M($\frac{1}{2}\,\frac{1}{2}$ 0) point of the Brillouin zone [8]. Hence, the Brillouin-zone centre modes of phase II arise from the Γ(0 0 0) and M($\frac{1}{2}\,\frac{1}{2}$ 0) points of phase I Brillouin zone. The compatibilities between the symmetries in the two phases are the following:

(i) Γ_1 and M_3 modes of phase I correspond to the two A_{1g} modes in phase II;
(ii) M_7 and M_5 modes have the B_{2g} and B_{1g} symmetries respectively; and
(iii) Γ_9 and the two M_9 modes are expected with the E_g symmetry.

The A_{1g} and E_g modes observed at 544 and 228 cm^{-1} correspond to the Γ_1 and Γ_9 modes respectively. The Γ_1 symmetry mode corresponds to a symmetric vibration of F_{ax} along the [0 0 1] direction and the Γ_9 mode corresponds to F_{ax} vibrations in the (0 0 1) plane. The other line with A_{1g} symmetry arises from the M_3 symmetry mode, which corresponds to AlF_6 octahedra librations around the tetragonal axis. This mode is condensed in phase II; its frequency cannot be compared to M_3 frequency calculated in the ideal structure. The B_{1g} mode at 451 cm^{-1} and the B_{2g} mode at 374 cm^{-1} are attributed to the M_5 and M_7 modes calculated at 498 and 426 cm^{-1} respectively. The second E_g mode measured at

354 cm^{-1} can be attributed to the M_9^2 mode calculated at 384 cm^{-1}; the last M_9 (M_9^1) mode is expected to have a low frequency and is not observed.

Table 2. Calculated phonon frequencies (cm^{-1}) of $KAlF_4$ at room temperature at the Γ, M and X points of the Brillouin zone for the tetragonal ideal structure. The model used for this calculation is a rigid-ion model involving 10 parameters [8]. The frequency of M_3 is imaginary ($i = \sqrt{-1}$), which formally reflects the fact that it is already condensed (phase II).

	Γ_4^1				Γ_{10}^1	
Γ_1	TO	LO	Γ_8	Γ_9	TO	LO
553	128	194	267	209	103	132
	493	500			214	223
	689	806			399	499
					658	731

X_1^1	X_3^1	X_4^1	X_5^1	X_6^1	X_7^1	X_8^1
163	7.6	116	206	241	85	140
491	107	333		287	269	402
636	395	654		645		668

M_1^1	M_3	M_4^1	M_5	M_6	M_7	M_9^1	M_{10}^1
483	421	266	498	92	426	11	133
695		660				384	247
							541

To summarize, the Raman scattering results are consistent with the calculated values. Among the observed Raman-active modes, only the M_3 mode is strongly dependent upon x; this is the mode responsible for the phase I–phase II transition observed at 280 °C in $RbAlF_4$ and which is shifted above the melting point (above 560 °C) in $KAlF_4$.

3.3. $K_{0.94}Rb_{0.06}AlF_4$ and $K_{0.91}Rb_{0.09}AlF_4$: phase III

The Raman spectra of $K_{1-x}Rb_xAlF_4$ with $x = 0.06$ and $x = 0.09$ present the same characteristics at low temperature and the same assignment is proposed.

According to the space group $P2_1/m$ as proposed by Launay *et al* [5], the Raman-active modes in phase III have the following symmetries:

$$17A_g + 13B_g.$$

Note that the a_{III}, b_{III}, c_{III} axes are almost parallel to the a_I, b_I, c_I axes respectively and so (almost) parallel to the X, Y, Z system chosen for the experimental analysis. However, the transition from a tetragonal to a monoclinic phase is responsible for the development of four domains in the low-temperature phase III with two possible orientations for the binary axis of the monoclinic phase. In the present case, the binary axis can be parallel to the a_I

or to the b_1 vectors [5]. The Raman tensors for these two possible orientations are reported in table 1. The A_g and B_g symmetry modes can be distinguished only by their presence or absence in the parallel geometries and in the XY geometry.

The Raman spectra collected in different polarizations for $K_{0.94}Rb_{0.06}AlF_4$ are given in figure 4 and the frequencies considered for the discussion are those of this compound.

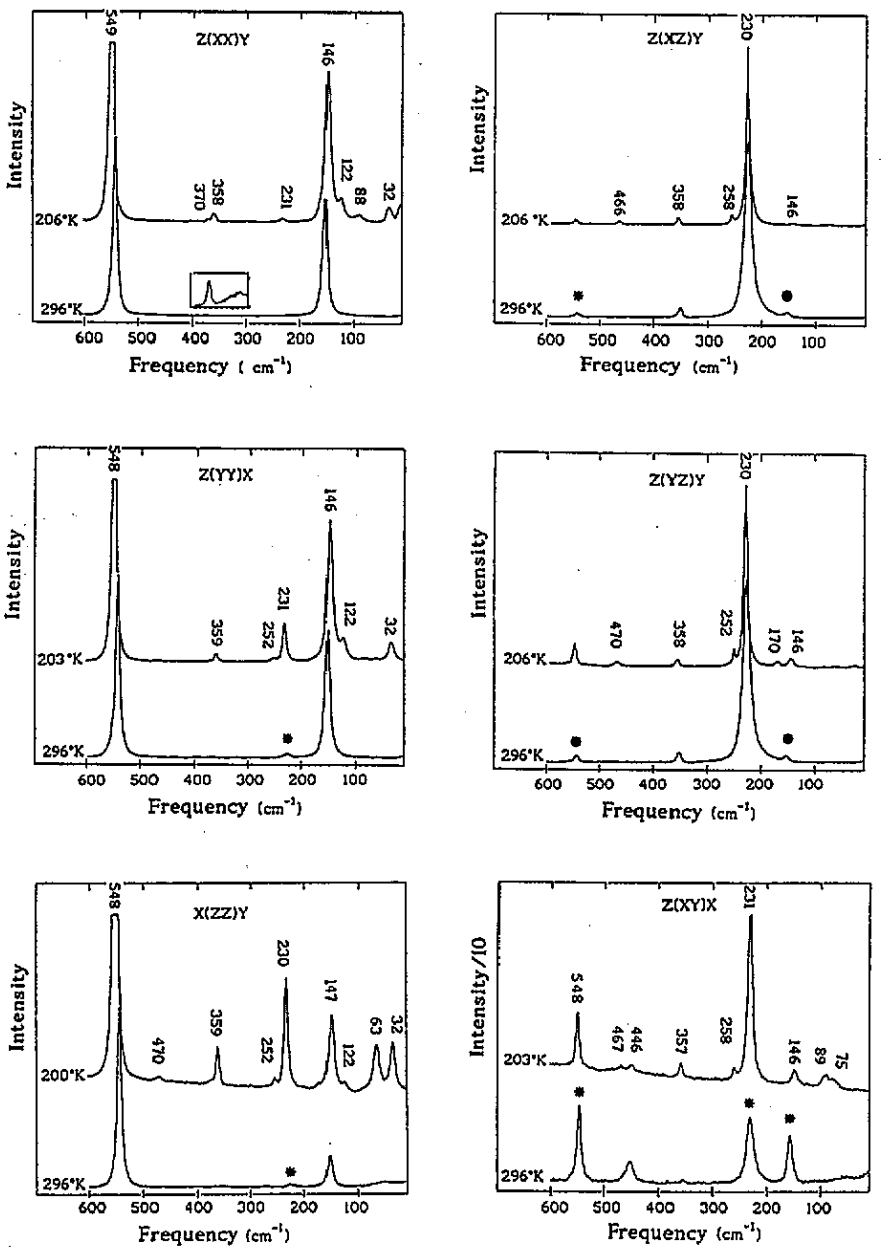

Figure 4. Raman spectra of $K_{0.94}Rb_{0.06}AlF_4$ collected in phase II (296 K) and in phase III (in the vicinity of 203 K) in the $Z(XX)Y$, $Z(YY)X$, $X(ZZ)Y$, $Z(XZ)Y$, $Z(YZ)Y$ and $Z(XY)X$ geometries. Asterisks indicate contamination due to intense lines active in another geometry.

3.3.1. A_g symmetry modes. Since there is a group–subgroup relationship between the phase II and phase III space groups, the A_{1g} lines of the former become A_g lines of the latter and they are observed with the same geometry. A surprising effect is the 'softening', in the phase III, of the low-frequency A_{1g} line of phase II. It is also noted that the intensityof the E_g line at 358 cm^{-1} at room temperature strongly grows in parallel configurations: they have also an A_g character. The mode measured at 370 cm^{-1} corresponding at room temperature to the B_{2g} mode is observed in XX and ZZ geometries, so its symmetry is A_g.

In other respects, a lot of new lines appear in parallel configurations. We can identify easily the symmetry of some of them. The lines at 32 and at 122 cm^{-1} (only observed in the XX, YY and ZZ geometries) and the line at 63 cm^{-1} (only detected in ZZ configuration) have the A_g symmetry. The line at 252 cm^{-1} observed in the YY, ZZ and YZ geometries is also A_g. At higher frequencies, a low-intensity mode at 470 cm^{-1} appears in ZZ and YZ configurations and so belongs to the A_g symmetry.

3.3.2. B_g symmetry modes. In the XY geometry, only the B_g symmetry modes should be observed. Because of contamination by intense A_g lines the experimental spectra show a lot of lines.

Among intense Raman lines already active at room temperature, a line at 231 cm^{-1} is still observed in XZ, YZ and XY configurations and so has a B_g character. On the other hand, in the XY polarization, its intensity grows a lot when the temperture decreases and so it can be supposed that a new line is superimposed. The E_g line at 358 cm^{-1} at room temperature is observed in all configurations at low temperature. A careful analysis reveals two lines: a line labelled L6 at 359 cm^{-1} with the A_g symmetry as previously mentioned and another labelled L7 at 357 cm^{-1} with B_g symmetry. The B_{1g} mode observed at 450 cm^{-1} at room temperature, becomes a B_g mode measured at 446 cm^{-1}, only observed in XY geometry.

The new lines at 75 cm^{-1} (observed only in the XY geometry), at 258 cm^{-1} (observed in XZ and XY configurations) and a very low-intensity line at 467 cm^{-1} (in the XY and XZ polarizations) also have the B_g symmetry.

3.3.3. Ambiguity of some lines. There are also some lines for which the attribution is more difficult to establish. For example, the line at 89 cm^{-1} is observed in XX and XY configurations. Its symmetry can be A_g and/or B_g. The line at 170 cm^{-1} is only observed in YZ geometry, which would not be enough to draw a conclusion. However (from subsections 3.3.1 and 3.3.2) it can be noted that the lines attributed to A_g symmetry modes are observed in the YZ geometries (see the 252 and 470 cm^{-1} lines) while the B_g ones are observed in the XZ geometry (see the 258 and 467 cm^{-1} lines); in other words, in our experiment on the sample with $x = 0.06$, it seems that the domains are mainly such that the twofold monoclinic axis is parallel to the X direction. With this remark, we can deduce that the line at 170 cm^{-1} corresponds to an A_g vibrational mode.

The Raman line frequencies of $K_{0.94}Rb_{0.06}AlF_4$ in the vicinity of 203 K are reported in table 3 with the geometry in which they are observed and with their symmetry.

3.3.4. Assignment to vibrational modes. Owing to the relationship between the lattices parameters in phase I and phase III, it can be deduced that the zone centre modes of phase III (Γ_{III} point) correspond to modes located at the Γ_I, M_I and X_I points of the Brillouin zone of the ideal phase I. The compatibility relations between the symmetries in phases I and III are described in table 4. The assignment proposed below relies on the use of this compatibility

Table 3. Frequencies (column 2) of the Raman lines of $K_{0.94}Rb_{0.06}AlF_4$ phase III measured at ~ 203 K. The Raman lines are labelled (column 1) according to decreasing frequencies. The geometry in which they are observed and the associated symmetry in the framework of the $P2_1/m$ space group are given in columns 3 and 4 respectively. An attribution based upon comparison with the calculated phonon spectrum of pure $KAlF_4$ is proposed in column 5. The attribution given in parentheses may be questionable due to the possible mixing in such a small frequency range.

lines	$\omega(cm^{-1})$	polarizations	symmetries	modes
L17	32	XX,YY,ZZ	A_g	(X_3^1, M_9^1)
L16	63	ZZ	A_g	(X_3^1, M_9^1)
L15	75	XY	B_g	(M_9^1, X_7^1)
L14	89	XX,XY	A_g, B_g	(M_9^1, X_7^1)
L13	122	XX,YY,ZZ	A_g	X_3^2
L12	146	XX,YY,ZZ,XZ,YZ	A_g	M_3
L11	170	YZ	A_g	X_1^1
L10	231	XX,YY,ZZ,XZ,YZ,XY	A_g, B_g	Γ_9, X_5
L9	252	YY,ZZ,YZ	A_g	X_7^2
L8	258	XZ,XY	B_g	X_7^2
L7	357	XZ,YZ,XY	B_g	M_9^2
L6	359	XX,YY,ZZ	A_g	(X_3^3, M_9^2)
L5	370	ZZ,YZ	A_g	M_7
L4	446	XY	B_g	M_5
L3	467	XZ,XY	B_g	X_1^2, M_1^1
L2	470	ZZ,YZ	A_g	X_1^2
L1	548	XX,YY,ZZ,XZ,YZ	A_g	Γ_1

Table 4. Compatibility relations between the symmetries in the ideal phase and the zone centre symmetries of the phase III (or IIIa) (space group $P2_1/m$) associated with the Raman-active modes.

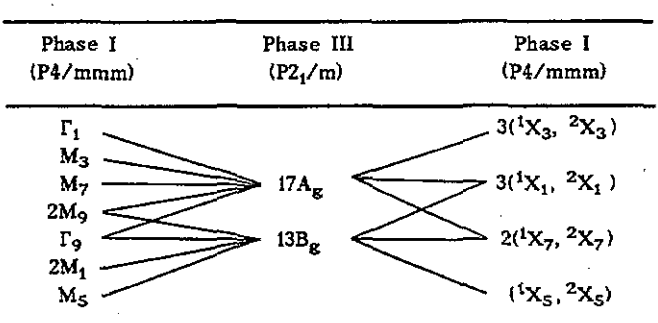

diagram together with the calculated values of the frequencies reported in table 2. The assignment is done for decreasing frequencies.

The highest frequency (line L1, table 3) with A_g symmetry unambiguously comes from the Γ_1 mode characteristic of this layer arrangement. The L2, L3 and L4 lines are observed in the same frequency range. Taking into account the symmetries, only the X_1^2 mode is consistent with the former, which has an A_g symmetry. The others, L3 and L4 with B_g symmetry, can be attributed to M_1^1, M_5 or X_1^2 modes (X_1 is a twofold degenerate mode and leads to A_g and B_g symmetry modes). As L4 keeps exactly the same characteristic

below and above the transition, it is attributed to the M_5 mode, like at room temperature. The M_7 mode, active in phase II, is assigned to the L5 line. The L6 line (A_g symmetry) and L7 line (B_g symmetry), only separated by 2 cm^{-1}, seem to arise from a splitting. The nearest calculated frequencies correspond to the M_9^2 and X_3^3 modes, both degenerate. The X_3 mode gives rise to two A_g symmetry modes. So, the L6 line arises from the X_3^3 or the M_9^2 mode and the L7 line comes from the degenerate M_9^2 mode. The L8 and L9 lines appear in a frequency range such that they have to be associated with the degenerate X_7^2 mode, which, consistently, should give rise in phase III to two modes with A_g and B_g symmetry. The L10 line, already active in phase II, is assigned to the Γ_9 mode. However, as mentioned above, the component with the B_g symmetry grows a lot in phase III: this phenomenon could also result from the emergence of two B_g symmetry modes corresponding to the degenerate X_5 mode in phase I. The new line L11, with A_g symmetry, is attributed to the X_1^1 mode. According to the attribution proposed in phase II, the L12 line arises from the M_3 mode whose condensation is responsible for the (virtual) phase I–phase II transition. The A_g symmetry of L12 in phase III is consistent with such an attribution. It must be noted, however, that this line undergoes an unexpected decrease of frequency at the phase II–phase III transition. This could attest to a structural rearrangement at this first-order transition.

At lower frequency, any correspondence between the symmetries in phase I and phase III is questionable owing to the soft character of several modes and to possible mixings. The L13 line with A_g symmetry probably comes from the X_3^2 mode. The L14 and L15 lines are attributed to the M_9^1 and/or X_7^1 mode because of their B_g symmetries. At least, L16 and L17 lines have A_g symmetry and they arise from the M_9^1 and/or X_3^1 mode.

So, the Raman spectra can be explained with the calculated spectrum in the framework of the space group proposed by Launay *et al* [5]. Figures 5(*a*) and (*b*) respectively show temperature behaviour of the Raman line frequencies of $K_{0.94}Rb_{0.06}AlF_4$ and $K_{0.91}Rb_{0.09}AlF_4$. It appears that several low-frequency modes have a soft character. Note that for $x = 0.09$, splitting of the X_7^2 modes, in the vicinity of the transition, is not observed. With regard to the behaviour of the $K_{0.85}Rb_{0.15}AlF_4$ compound (see below), an intermediate phase may already exist in $K_{0.91}Rb_{0.09}AlF_4$. This remark is also supported by recent x-ray diffraction studies on single crystals [11].

3.4. $K_{0.85}Rb_{0.15}AlF_4$: phase IIIa and phase IIIb

The Raman spectra collected in different polarizations are given in figure 6. It appears that the three different temperatures give three different Raman spectra and so are evidence for three different phases. They are denoted phase II at room temperature, phase IIIb and phase IIIa at low temperature. The spectra obtained in phase IIIa are similar to the spectra collected in phase III of $K_{0.94}Rb_{0.06}AlF_4$ (figure 4). So, we can reasonably identify this phase IIIa with the phase III of this compound. The spectra recorded in phase IIIb exhibit extra lines with respect to those of phase II, but most of the lines observed in phase IIIa are not observed in phase IIIb. The origin of these lines is discussed below.

3.4.1. Phase IIIb. With respect to phase II, in phase IIIb four additional lines are observed (figure 6): two lines in the $X(ZZ)Y$ geometry at 41 cm^{-1} (broad) and 360 cm^{-1} (with low intensity), a line at 256 cm^{-1} in the $Z(YZ)X$ and $Z(XZ)Y$ polarizations and a line with a very low intensity at 471 cm^{-1} in $Z(XZ)Y$ geometry.

The existence of this new phase IIIb in the mixed compounds $K_{1-x}Rb_xAlF_4$ has never been reported before. In the following, an attempt is made to assign the Raman spectra and to propose a space group for this phase.

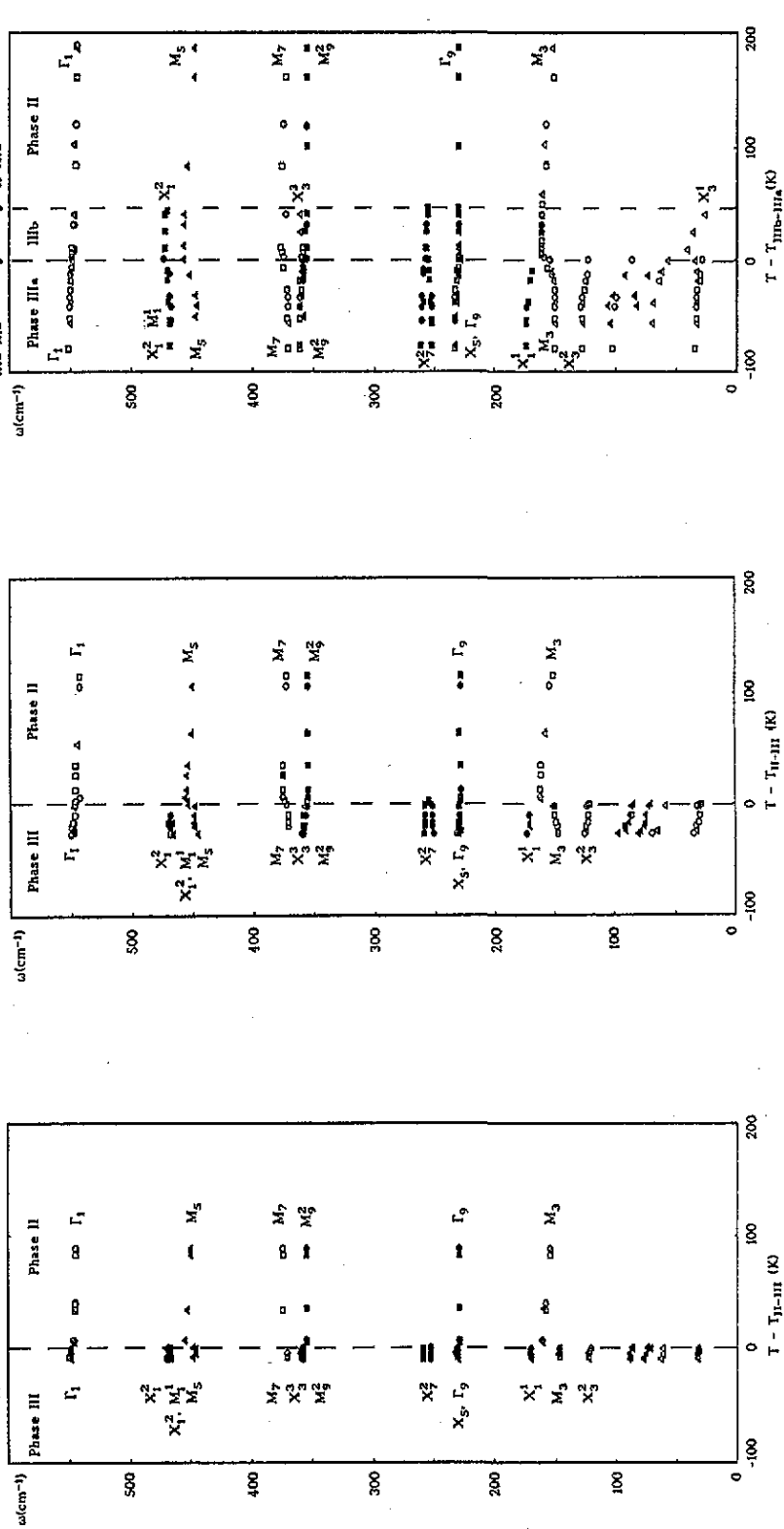

Figure 5. Temperature behaviour of the Raman-active mode frequencies of $K_{0.94}Rb_{0.06}AlF_4$ (*a*), $K_{0.91}Rb_{0.09}AlF_4$ (*b*) and $K_{0.85}Rb_{0.15}AlF_4$ (*c*) and the proposed assignment to the vibrational modes in the aristotypic phase. The symbols correspond to the *XX* (□), *YY* (○), *ZZ*, (△), *XZ*, (■), *YZ*, (●) and *XY*, (▲) geometries.

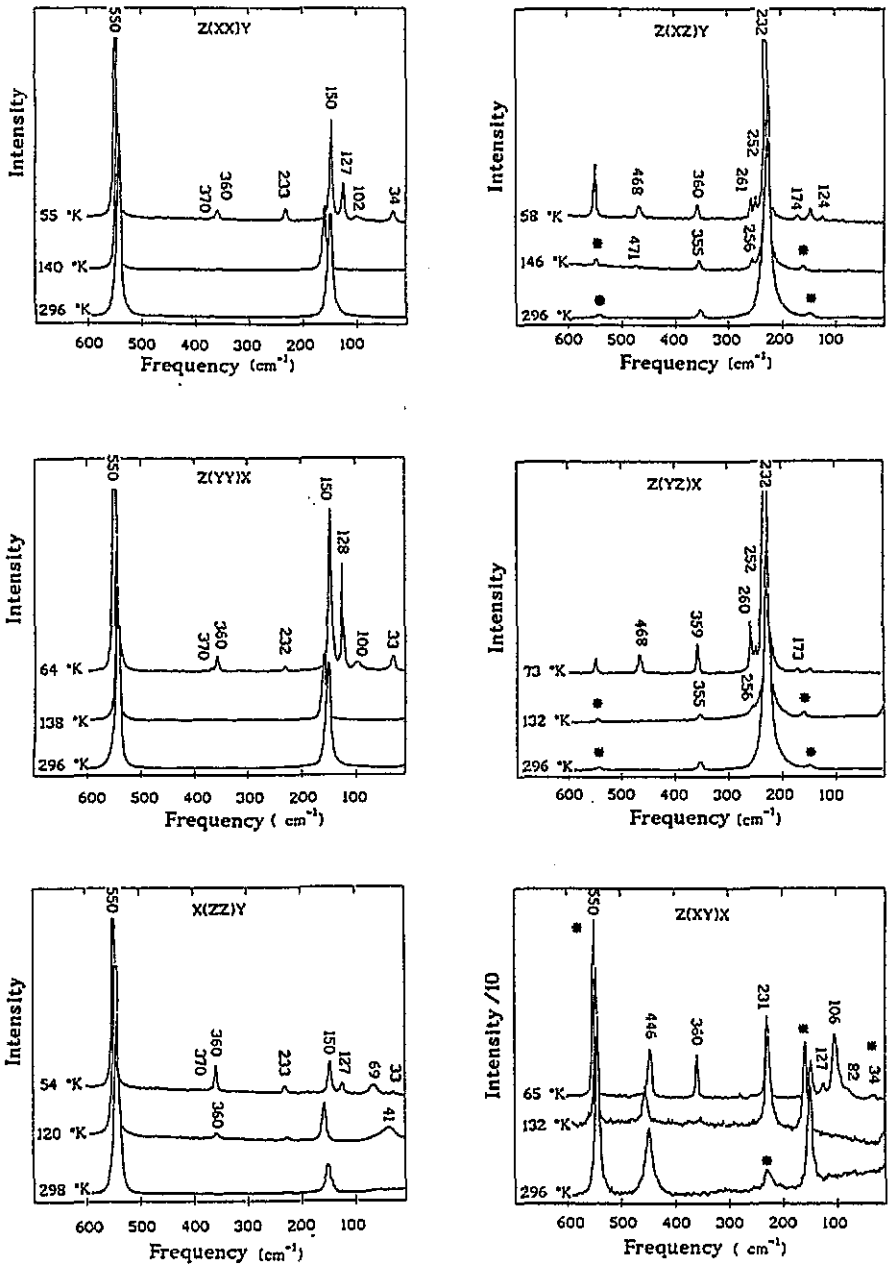

Figure 6. Raman spectra of $K_{0.85}Rb_{0.15}AlF_4$ collected in different phases in the $Z(XX)Y$, $Z(YY)X$, $X(ZZ)Y$, $Z(XZ)Y$, $Z(YZ)X$ and $Z(XY)X$ geometries. Asterisks indicate contamination due to intense lines active in another geometry.

Structurally, the transitions in this kind of compound usually come from condensation of low-frequency X_3 or M_9 modes. In particular, phase III (or IIIa) can be imputed to the condensation of the two components of the degenerate X_3^1 mode ('in-phase' tilts of successive AlF_6 octahedra around $[1\,0\,0]_I$ and $[0\,1\,0]_I$ directions with translation of the

monovalent cations in $[0\,0\,1]_I$ direction) plus one of the two components of the degenerate M_9^1 mode ('alternated' tilts of AlF_6 octahedra). It is reasonable to think that phase IIIb is related to the condensation of one or two components of these two modes. The Raman spectra predicted under these hypotheses are discussed below.

(i) Condensation of M_9 mode. In the case of the condensation of the M_9 mode, the Raman-active modes (coming from M points of the ideal tetragonal Brillouin zone) would be the two M_1 modes (calculated at 483 and 695 cm^{-1} in pure $KAlF_4$; table 2) and the two M_9 modes (11 and 384 cm^{-1}). None of these modes could explain the experimental line observed at 256 cm^{-1}. Moreover, studies of phase III (or IIIa) of $K_{0.94}Rb_{0.06}AlF_4$ show that such a line arises from the X_7^2 modes. This one corresponds to equatorial fluorine ion vibrations in the layer plane and its frequency remains almost the same in all these compounds: for $RbAlF_4$, in its low-temperature phase, this mode has been identified and measured at 251 cm^{-1} [12, 13]. Then, a phase transition due to the condensation of the M_9 mode (one or two components) would not lead to Raman spectra consistent with those observed in phase IIIb.

(ii) Condensation of X_3 mode. In the case of the condensation of X_3, the phase II–phase IIIb transition would be similar to the phase II–phase III_{Rb} transition of pure $RbAlF_4$ [13]. The space group of $RbAlF_4$ in phase III_{Rb} is *Pmmn* and the system can be summarized by $a_p^+b^0c^+$ or $a_p^+b_p^+c^+$ [2]. In this framework, the symmetries of the Raman-active modes in phase IIIb would be the following:

$$9A_g + 5B_{1g} + 8B_{2g} + 8B_{3g}.$$

The Raman tensors are reported in table 1; in this case the X, Y, Z axes chosen for the experimental analysis are parallel to the orthorhombic crystallographic axes but two kinds of domains ($X \parallel a_{III}$ and $Y \parallel b_{III}$ or $X \parallel b_{III}$ and $Y \parallel a_{III}$) may appear. These modes arise from modes located at the Γ_I, M_I and X_I points of the Brillouin zone of phase I. The compatibility relations between the symmetries in phase I and the zone centre symmetries of phase IIIb are given in table 5.

Table 5. Compatibility relations between the symmetries in the ideal phase and the zone centre symmetries of the phase IIIb (*Pmmn*) for the Raman-active modes.

Phase I (P4/mmm)	Phase IIIb (Pmmn)	Phase I (P4/mmm)
Γ_1, M_3, M_7	$9A_g$	$3(^1X_3, {}^2X_3)$
$2M_1$, M_5	$5B_{1g}$	$(^1X_5, {}^2X_5)$
Γ_9	$8B_{2g}$	$3(^1X_1, {}^2X_1)$
$2M_9$	$8B_{3g}$	$2(^1X_7, {}^2X_7)$

Modes already active at room temperature are unambiguouosly identified. The new line at 471 cm^{-1} observed in $Z(XZ)Y$ geometry with very low intensity has B_{2g} or B_{3g} symmetry. It can be attributed to the X_1^2 mode calculated at 491 cm^{-1} (in pure $KAlF_4$). The

Table 6. Frequencies of the Raman lines of $K_{0.85}Rb_{0.15}AlF_4$ phase IIIb measured at $\sim$ 120 K (*a*) and at $\sim$ 64 K (*b*) together with the geometries in which they are observed and the associated symmetry in the framework of the *Pmmn* (*a*) and $P2_1/m$ (*b*) space groups. An attribution based upon comparison with the calculated phonon spectrum of pure $KAlF_4$ is proposed in the last column. The attribution given in parentheses may be questionable due to the possible mixing in such a small frequency range.

$\omega(cm^{-1})$	polarizations	symmetries	modes
41	ZZ	A_g	X_3^1
161	XX,YY,ZZ	A_g	M_3
229	XZ,YZ,XY	B_{2g}, B_{3g}	Γ_9 ,(X_5)
256	XZ,YZ	B_{2g}, B_{3g}	X_7^2
355	XZ,YZ	B_{2g}, B_{3g}	M_9^2
360	ZZ	A_g	X_3^3
374	XX,YY	A_g	M_7
456	XY	B_{1g}	M_5
471	XZ	B_{2g}, B_{3g}	X_1^2
547	XX,YY,ZZ	A_g	Γ_1

lines	$\omega(cm^{-1})$	polarizations	symmetries	modes
L18	33	XX,YY,ZZ	A_g	(X_3^1)
L17	68	ZZ	A_g	(X_3^1)
L16	82	XY	B_g	(M_9^1, X_7^1)
L15	100	XX,YY	A_g	(M_9^1, X_7^1)
L14	106	XY	B_g	(M_9^1, X_7^1)
L13	128	XX,YY,ZZ,XZ	A_g	X_3^2
L12	150	XX,YY,ZZ,XZ,YZ	A_g	M_3
L11	174	XZ,YZ	A_g B_g	X_1^1
L10	232	XX,YY,ZZ,XZ,YZ,XY	A_g B_g	Γ_9 , X_5
L9	252	XZ,YZ	A_g B_g	X_7^2
L8	260	XZ,YZ	A_g B_g	X_7^2
L7	359	XZ,YZ,XY	A_g B_g	(M_9^2)
L6	360	XX,YY,ZZ,XZ	A_g	(X_3^3)
L5	370	XX,YY,ZZ	A_g	M_7
L4	446	XY	B_g	M_5
L3	467	XZ,YZ	A_g B_g	X_1^2, M_1^1
L2	468	XZ,YZ	A_g B_g	X_1^2
L1	550	XX,YY,ZZ,XZ,YZ	A_g	Γ_1

line measured at 360 cm^{-1} with A_g symmetry can only come from the second component of the X_3^3 mode since the other modes with this symmetry have already been attributed. The line at 256 cm^{-1}, with B_{2g} or B_{3g} symmetry, arises from the X_7^2 mode. The expected splitting of this mode is not observed, however (figure 5(*c*)). A broad line at 41 cm^{-1} is observed in $X(ZZ)Y$ geometry and so it belongs to the A_g symmetry. This line has a

soft character and it is attributed to the X_3^1 mode. However, the X_3^1 mode is degenerate in phase II and so for $RbAlF_4$, as expected, it gives rise to two lines below 50 cm^{-1}. Owing to its very broad character in $K_{0.85}Rb_{0.15}AlF_4$, the 41 cm^{-1} line could include two lines.

So it appears that the Raman spectra in phase IIIb can be explained under the hypothesis that the II–IIIb phase transition results from the condensation of X_3; the corresponding space group is *Pmmn*. The temperature behaviour of the Raman-active mode frequencies of $K_{0.85}Rb_{0.15}AlF_4$ is shown in figure 5(*c*). In table 6(*a*) are reported the frequencies measured in the vicinity of 120 K, the geometry for their observation, their symmetry and the assignment proposed.

3.4.2. Phase IIIa. The spectra collected in phase IIIa are similar to those recorded in phase III for $K_{0.94}Rb_{0.06}AlF_4$. Let us note, however, the simultaneous presence of lines at 252 cm^{-1} (L9; table 6(*b*)) and at 260 cm^{-1} (L8) in the $Z(XZ)Y$ and $Z(YZ)X$ geometries. Hence, unlike phase III (or IIIa) of the other compounds studied, phase IIIa presents monoclinic domains with binary axes parallel to the X and Y experimental directions as well. Such an organization may result from the fact that for x greater than 0.09, phase IIIb is issued from an orthorhombic phase made up of two domains turned by 90° around the c_I axis.

The Raman line frequencies of $K_{0.85}Rb_{0.15}AlF_4$ in different geometries in the vicinity of 64 K with their symmetries and the proposed assignment to vibration modes are summarized in table 6(*b*). For the modes with frequencies higher than 150 cm^{-1}, the same assignment as for x less than 0.09 can be used (table 6(*b*)). Below about 100 cm^{-1} six lines are expected in phase IIIa: four with A_g symmetry coming from the splitting of X_3^1, M_9^1 and X_7^1 modes and two lines with B_g symmetry arising from M_9^1 and X_7^1 modes. The L14 and L16 lines are attributed to the M_9^1 or X_7^1 modes because of their B_g symmetry. The broad line at 41 cm^{-1} in phase IIIb seems to split into two lines with very close frequencies in the vicinity of the phase IIIb–phase IIIa transition (L17 and L18 lines; table 6(*b*)), and so the frequencies of these lines are not estimated accurately. This fact can explain the difference of the frequencies measured in the (XX, YY) and in the ZZ geometries for the L18 line in phase IIIa (figure 5(*c*)). Also, these two lines could be attributed to the two components of the doubly degenerate X_3^1 mode, which support the remark given in section 3.4.1 about the broad character of the 41 cm^{-1} line. Note that the L17 line exhibits a soft mode behaviour while the L18 line is almost temperature-independent. However, the soft character of several low-frequency modes and possible 'mixings' of modes make assignment in this frequency range questionable.

3.4.3. Discussion. The Raman scattering investigation discussed here evidences the existence of a new phase in the phase diagram of $K_{1-x}Rb_xAlF_4$. The spectra cannot be interpreted with condensation of an M_9 mode. On the other hand, an assignment to vibration modes is possible in the space group *Pmmn*, i.e. the phase IIIa–phase IIIb transition could arise from condensation of the X_3^1 mode like in pure $RbAlF_4$. The proposed assignment is consistent with the one proposed in phase II and in phase IIIa. The X_7^2 and X_3^1 are not split in phase IIIb but birefringence studies [14] unambiguously show, owing to the presence of domains, that the tetragonal symmetry is lost. The study of this compound in the new phase IIIb also reveals the soft character of several low-frequency A_g modes.

4. Conclusion

An assignment to vibration modes of most of the experimental Raman lines, on a basis

of calculation of phonon spectra in the ideal phase of pure $KAlF_4$, has been proposed for all the $K_{1-x}Rb_xAlF_4$ compounds with $x \leqslant 0.15$. The spectra collected in the low-temperature phase (phase IIIa) are still consistent with the $P2_1/m$ symmetry. The phase II–phase IIIa transition could arise from condensation of the two components of the X_3^1 mode plus condensation of one component of the M_9^1 mode. Moreover, a new phase IIIb has been evidenced in $K_{0.85}Rb_{0.15}AlF_4$. It has been shown that the Raman spectra collected in this new phase could be explained under the hypothesis of the condensation of the X_3^1 mode like in the pure compound $RbAlF_4$. This new information helps to complete the assignment of the low-frequency vibrational mode in phase IIIa.

In this Raman scattering study, the frequencies of some vibrational modes never obtained before have been measured: M_5, M_7, M_9 and several modes at the X point of the Brillouin zone. These new values make it possible to get better values of the force constants describing the inter-ionic interactions and a better description of the phonon spectrum could be obtained. This is useful to predict the phonon spectra of isomorphous materials and the phase transitions therein.

These $K_{1-x}Rb_xAlF_4$ compounds exhibit a phase diagram with four different phases in the concentration range x less than 0.15. Two phase transitions can be imputed to the condensation of two modes (X_3^1 and M_9^1) with degeneracy 2. One can expect to explain such a phase diagram with a Landau free energy; the sequence of the phase transitions together with their x dependence may lead to a good estimation of the phenomenological parameters of the free energy. The main interest comes from the fact that a third phase transition in this phase diagram exhibits martensitic behaviour.

Acknowledgments

The authors wish to thank Professor M Rousseau for fruitful discussions and G Niesseron for growing the single crystals. This work has benefited by a financial support from the DRCI of the CNRS for the constitution of European Network of Laboratories.

References

[1] Brosset C 1937 *Z. Anorg. Allg. Chem.* **235** 139–47
[2] Bulou A and Nouet J 1982 *J. Phys. C: Solid State Phys.* **15** 183–96
[3] Launay J M, Bulou A, Hewat A W, Gibaud A, Laval J Y and Nouet J 1985 *J. Physique* **46** 173–84
[4] Bulou A, Gibaud A, Launay C, Debieche M, Rousseau M, Nouet J and Hennion B 1989 *Phase Transitions* **14** 47–53
[5] Launay C, Bulou A and Nouet J 1987 *Solid State Commun.* **69** 539–41
[6] Glazer A M 1975 *Acta Crystallogr.* A **31** 756–62
[7] Fourquet J L, Plet F, Courbion G, Bulou A and De Pape R 1979 *Rev. Chim. Minér* **16** 490–500
[8] Bulou A 1985 *Thesis* Le Mans
[9] Bulou A, Rousseau M, Nouet J, Loyzance P L, Mokhlisse R and Couzi M 1983 *J. Phys. C: Solid State Phys.* **16** 4527–537
[10] Heger G, Geller R and Babel D 1971 *Solid State Commun.* **9** 335–40
[11] Brunet F, Gibaud A, Ridou C and Nouet J 1991 *Ferroelectrics* **124** 315–20
[12] Ganot F, Papin M, Bulou A and Moch P 1991 *Ferroelectrics* **124** 321–6
[13] Bulou A, Rousseau M, Nouet J and Hennion B 1989 *J. Phys.: Condens. Matter* **1** 4553–83
[14] Farhi R, Sommer D and Kleemann W 1991 *Ferroelectrics* **124** 327–32